Short-term stability of patterns in intracavity vectorial second-harmonic generation

C. Etrich, D. Michaelis, U. Peschel, and F. Lederer
Institut für Festkörpertheorie und Theoretische Optik, Friedrich-Schiller-Universität Jena, Max-Wien-Platz 1, 07743 Jena, Germany
(Received 8 April 1998)

We examine how patterns develop from the point where the plane wave modulational instability sets in. In particular, it is found that in a certain domain of parameter space square patterns bifurcate stably from this point. [S1063-651X(98)06709-9]

PACS number(s): 42.65.Sf, 42.65.Ky

Quadratically nonlinear processes have attracted a great deal of attention in recent years because of a deeper interest in the nonlinear dynamics of the coupled waves involved, especially if transverse effects are included. Among basic configurations are externally driven planar resonators filled with a quadratically nonlinear medium. If only two frequencies, i.e., the fundamental and second harmonic, are concerned, the driving field is at the fundamental in intracavity second harmonic generation (up-conversion, SHG) whereas it is at the second harmonic in optical parametric oscillators (down-conversion, OPO's). Fundamental transverse effects are the formation of periodic patterns [1–5] and solitary waves or localized structures [6–9]. Most investigations concentrated on the scalar case where only two waves are considered. In both configurations, SHG and OPO, the existence of hexagonal patterns [1] and localized structures [6–8] was demonstrated. The emergence of roll patterns in the OPO was extensively studied in Ref. [1].

Here we consider the case of vectorial intracavity SHG with the system driven by the two orthogonally polarized fundamental fields at the same frequency. The aim of this work is to analyze which periodic patterns evolve stably from the point where the plane wave modulational instability sets in on the symmetric branch (equal fundamental fields). This is done by means of amplitude equations from a multiple scale expansion with respect to this point. Despite the complexity of the evolution equations, it is possible to find them analytically. The main emphasis is on square patterns. In a certain domain of parameter space they evolve stably from the point where the modulational instability sets in, instead of roll patterns. In optics, stable square patterns were observed in a polarization instability device (Kerr slice) [10], and unstable ones were calculated in Ref. [11]. Finally we point out the similarities with the OPO (scalar), which is also shown to display square patterns.

We assume the system to be highly resonant for the three fields at two frequencies, and apply a mean field theory. Then the appropriately scaled evolution equations for the transmitted fields A_1, A_2, and B of the two fundamental and the second harmonics are derived as

$$
\begin{aligned}
&i\frac{\partial A_1}{\partial T}+(L+\Delta_A+i)A_1+A_2^*B=E,\\
&i\frac{\partial A_2}{\partial T}+(L+\Delta_A+i)A_2+A_1^*B=E,\\
&i\frac{\partial B}{\partial T}+(\alpha L+\Delta_B+i\gamma)B+A_1A_2=0,
\end{aligned}
\tag{1}
$$

where $L=(\partial^2/\partial X^2)+(\partial^2/\partial Y^2)$, T denotes the time, X and Y the transverse coordinates, Δ_A and Δ_B are the detunings of the fields from the corresponding resonances, γ is the ratio of the photon lifetimes, and α half the ratio of the refractive indices correponding to the fundamental and second harmonics. Throughout this analysis we assume that $\alpha=\frac{1}{2}$, which is a reasonable assumption. The symmetric input at the fundamental frequency is denoted by E.

First the homogeneous steady state or plane wave solutions A_{n0}, $n=1$ and 2, and B_0 of Eqs. (1) are considered. Equating the derivatives to zero and starting at $E=0$ yields a symmetric branch with $A_{10}=A_{20}$ which is the same as in the case of scalar SHG. To determine the stability of this branch we substitute $A_n=A_{n0}+\delta A_n\exp(\lambda T+i\mathbf{k}\cdot\mathbf{R})$, $n=1$ and 2, and $B=B_0+\delta B\exp(\lambda T+i\mathbf{k}\cdot\mathbf{R})$, with $\mathbf{k}=(k_X,k_Y)$, into Eqs. (1), and linearize with respect to δA_n, δB. This gives a characteristic equation of the linear problem which is a product of a quartic and a quadratic in λ. Critical points are marked by $\mathrm{Re}\lambda=0$. For the solution of the quartic we refer to Ref. [5]. In particular, for $\mathbf{k}=\mathbf{0}$ the symmetric branch may destabilize and stabilize at a pair of limit points. This is not considered here. One solution of the quadratic has always negative $\mathrm{Re}\lambda$, the other is

$$
\lambda=-1+\sqrt{|B_0|^2-(k^2-\Delta_A)^2}. \tag{2}
$$

For $k=0$ this yields a steady bifurcation where $|B_0|^2=\Delta_A^2+1$. This symmetry breaking bifurcation leads to asymmetric branches with $A_{10}\neq A_{20}$ [see Fig. 1(a) for a bifurcation diagram in terms of the control parameter E]. The modulational instability sets in where $|B_0|^2=1$, which corresponds to a critical value $E_c^2=2(\gamma-\Delta_A\Delta_B)+(\Delta_A^2+2)\sqrt{\Delta_B^2+\gamma^2}$. The critical wave number is $k_c^2=\Delta_A$, indicating that this modulational instability exists only for $\Delta_A>0$ (cf. also Refs. [12,13]). The fields at this point are

$$
A_{10}=A_{20}=\frac{1}{E_c}[\Delta_A\sqrt{\Delta_B^2+\gamma^2}-\Delta_B-i(\gamma+\sqrt{\Delta_B^2+\gamma^2})],
$$

$$
B_0=-\frac{A_{10}^2}{\Delta_B+i\gamma}. \tag{3}
$$

Here we focus on the point where the modulational instability sets in. To describe the dynamics near this point a

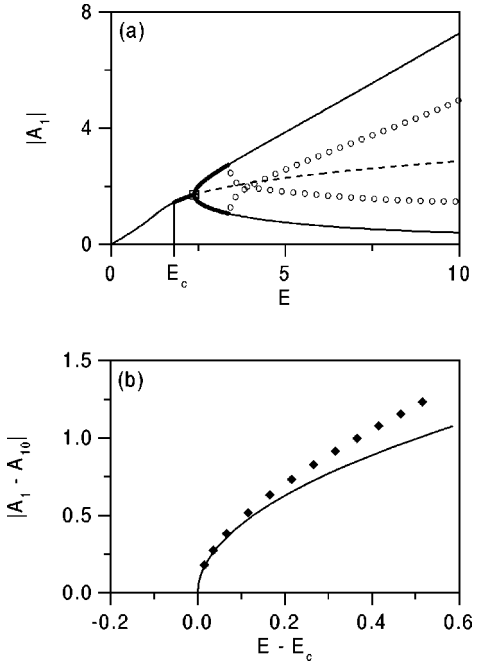

FIG. 1. (a) Bifurcation diagram displaying the modulus of one fundamental vs the control paramater E. Thin solid and dashed lines refer to stable and unstable plane wave solutions, respectively. Bold solid lines refer to modulationally unstable plane wave solutions. Open dots mark the amplitude at the center of unstable one-dimensional localized structures (stripes). The square marks the symmetry breaking bifurcation. (b) Relative maximum amplitudes of roll patterns (rhombs) compared to solutions from Eq. (9a) (solid line) with period $2\pi/k_c$ and bifurcating at $E=E_c$ [A_{10} from Eq. (3), $\Delta_A=1$, $\Delta_B=2$, and $\gamma=0.5$].

multiple scale analysis is performed. Assuming Δ_A of $O(1)$ and considering small deviations $E=E_c+\epsilon^2 E_2$ with $E_2=\pm 1$, the expansions

$$A_1=A_{10}+\epsilon A_{11}+\epsilon^2 A_{12}+\epsilon^3 A_{13}+\cdots,$$

$$A_2=A_{20}+\epsilon A_{21}+\epsilon^2 A_{22}+\epsilon^3 A_{23}+\cdots,$$

$$B=B_0+\epsilon B_1+\epsilon^2 B_2+\epsilon^3 B_3+\cdots \tag{4}$$

are substituted into Eqs. (1). Taking into account two wave vectors $\mathbf{k}_j$, with $k_j=k_c$ and $j=1$ and 2, which describes rhombic patterns, the solution at order $O(\epsilon)$ is

$$A_{11}=-A_{21}$$

$$=Fe^{i\mathbf{k}_1\cdot\mathbf{R}}-iB_0F^*e^{-i\mathbf{k}_1\cdot\mathbf{R}}$$

$$+Ge^{i\mathbf{k}_2\cdot\mathbf{R}}-iB_0G^*e^{-i\mathbf{k}_2\cdot\mathbf{R}},$$

$$B_1=0. \tag{5}$$

The coefficients F and G are functions of the slow variables $t=\epsilon^2 T$, $x_j=\epsilon X_j$, and $y_j=\sqrt{\epsilon}Y_j$ where the coordinates X_j and Y_j are parallel and perpendicular to the wave vectors $\mathbf{k}_j$, $j=1$ and 2, respectively. The angle between $\mathbf{k}_1$ and $\mathbf{k}_2$ should obey $\theta\gg\sqrt{\epsilon}$. The scaling of the slow variables becomes obvious if Eq. (2) is expanded around the critical point. For example, for one wave vector $\mathbf{k}=(k_c,0)$, substituting $E=E_c+\delta E$, $k_X=k_c+\delta k_X$, and $k_Y=\delta k_Y$ into Eq. (2) gives

$$\lambda=\frac{2E_c\delta E}{2E_c^2-\Delta_A^2\sqrt{\Delta_B^2+\gamma^2}}-\frac{1}{2}(2k_c\delta k_X+\delta k_Y^2)^2, \tag{6}$$

which implies above scaling if $\delta E\propto\epsilon^2$. Finally, at $O(\epsilon^3)$ a solvability condition yields the following amplitude or Newell-Whitehead-Segal equations for rhombs which contain the special case of rolls:

$$\frac{\partial F}{\partial t}=\beta_0E_2F-[(2\beta_1+\beta_2)|F|^2+2(\beta_1+\beta_3+\beta_4)|G|^2]F$$

$$-\frac{1}{2}\left(2ik_c\frac{\partial}{\partial x_1}+\frac{\partial^2}{\partial y_1^2}\right)^2F,$$

$$\frac{\partial G}{\partial t}=\beta_0E_2G-[(2\beta_1+\beta_2)|G|^2+2(\beta_1+\beta_3+\beta_4)|F|^2]G$$

$$-\frac{1}{2}\left(2ik_c\frac{\partial}{\partial x_2}+\frac{\partial^2}{\partial y_2^2}\right)^2G, \tag{7}$$

where the positive constants β_j are

$$\beta_0=\frac{2E_c}{(\Delta_A^2+4)\sqrt{\Delta_B^2+\gamma^2}+4(\gamma-\Delta_A\Delta_B)},$$

$$\beta_j=\frac{2\sqrt{\Delta_B^2+\gamma^2}+\gamma(\Delta_A^{(j)2}+2)}{\Delta_A^{(j)2}(\Delta_B^{(j)2}+\gamma^2)+4(\Delta_B^2+\gamma^2)+4\sqrt{\Delta_B^2+\gamma^2}(\gamma-\Delta_A^{(j)}\Delta_B^{(j)})}, \quad j=1,2,3,4, \tag{8}$$

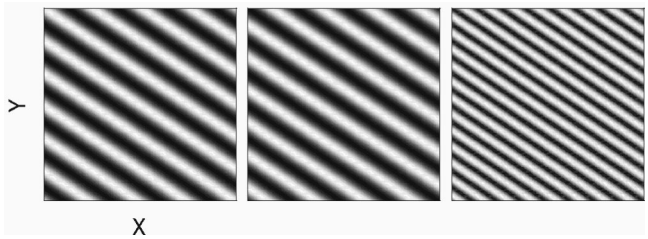

FIG. 2. Moduli of the two fundamental and second harmonics (from left to right) of a roll pattern for $\Delta_A=1$, $\Delta_B=2$, $\gamma=0.5$, and $E=2.2$ ($E_c=1.785$). The scale of the second harmonic is overemphasized for clarity. The computing window is 45.3 $\times$45.3 on a 64$\times$64 grid.

with $\Delta_A^{(1)}=\Delta_A$, $\Delta_B^{(1)}=\Delta_B$, $\Delta_A^{(2)}=\Delta_A-4k_c^2$, $\Delta_B^{(2)}=\Delta_B-2k_c^2$, $\Delta_A^{(3)}=\Delta_A-2k_c^2(1+\cos\theta)$, $\Delta_B^{(3)}=\Delta_B-k_c^2(1+\cos\theta)$, $\Delta_A^{(4)}=\Delta_A-2k_c^2(1-\cos\theta)$, and $\Delta_B^{(4)}=\Delta_B-k_c^2(1-\cos\theta)$. Patterns selected at the stage described by Eqs. (7) correspond to the nontrivial stable fixed points of these equations. The nontrivial fixed points are

$$|F|^2=\frac{\beta_0 E_2}{2\beta_1+\beta_2},\quad G=0, \tag{9a}$$

$$|G|^2=\frac{\beta_0 E_2}{2\beta_1+\beta_2},\quad F=0$$

$$|F|^2=|G|^2=\frac{\beta_0 E_2}{4\beta_1+\beta_2+2(\beta_3+\beta_4)}, \tag{9b}$$

which correspond to roll and rhombic patterns, respectively. In order to have nontrivial solutions $E_2=1$ is required, since the constants β_j are positive, i.e., the bifurcations are supercritical.

Here we examine the short-term stability of uniform patterns with respect to homogeneous perturbations. Linearizing Eqs. (7) around the roll solutions, the corresponding characteristic equation has the following solutions:

$$\lambda_1=0,\quad \lambda_2=-2\beta_0 E_2,$$

$$\lambda_3=\lambda_4=\beta_0 E_2\frac{\beta_2-2(\beta_3+\beta_4)}{2\beta_1+\beta_2}. \tag{10}$$

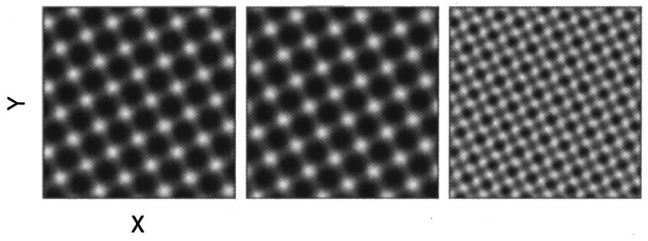

FIG. 3. Moduli of the two fundamental and second harmonics (from left to right) of a square pattern for $\Delta_A=1.5$, $\Delta_B=2$, $\gamma=0.5$, and $E=2.4$ ($E_c=1.939$). The scale of the second harmonic is overemphasized for clarity. The computing window is 37$\times$37 on a 64$\times$64 grid.

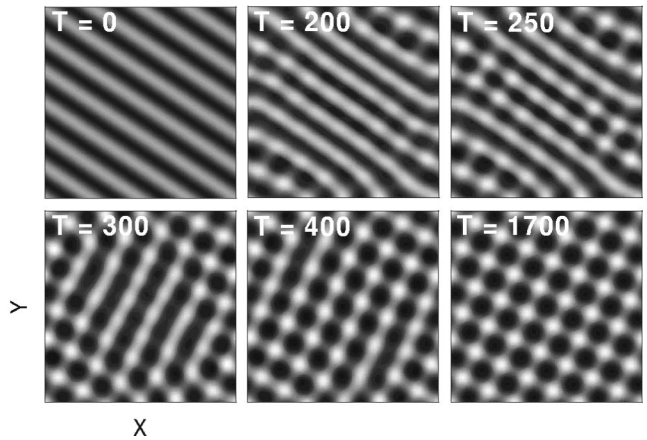

FIG. 4. Modulus of one fundamental displaying the decay of a roll pattern for $\Delta_A=1.5$, $\Delta_B=2$, $\gamma=0.5$, and $E=2.4$. The computing window is 37$\times$37 on a 64$\times$64 grid. A 128$\times$128 grid gives the same result.

The solution λ_1 is due to a phase invariance of the expressions given in Eqs. (9a). The solution λ_2 is always negative. If $\beta_2<2(\beta_3+\beta_4)$ roll patterns bifurcate stably from the critical point [cf. Fig. 1(b) for a bifurcation diagram in terms of E, and Fig. 2 for an example]. If $\beta_2>2(\beta_3+\beta_4)$ the solutions $\lambda_{3,4}$ describe the growth of the zero component of a roll solution [cf. Eq. (9a)]. In this case roll patterns bifurcate unstably. Since we find that the growth rate $\lambda_{3,4}$ is maximal for $\theta=\pi/2$, we expect square patterns to evolve near the critical point. Linearizing Eqs. (7) with respect to Eq. (9b) shows that squares emanate stably where roll patterns bifurcate unstably. Figure 3 displays an example of a stable square pattern which evolved from a randomly perturbed plane wave background, and Fig. 4 shows the decay of an unstable roll pattern from Eqs. (9a) into a square pattern. Unlike roll patterns, square patterns prevail only in a relatively narrow stability window, increasing the control parameter E from its critical value. As indicated by Eq. (5), the fundamental A_1 is maximal where A_2 is minimal, and vice versa, while the second harmonic B makes no contribution at this order (cf. Figs. 2 and 3). We find squares existing only for $\Delta_B>0$.

It should be noted that the case of hexagon patterns is included in above analysis ($\theta=\pi/3$). Starting with

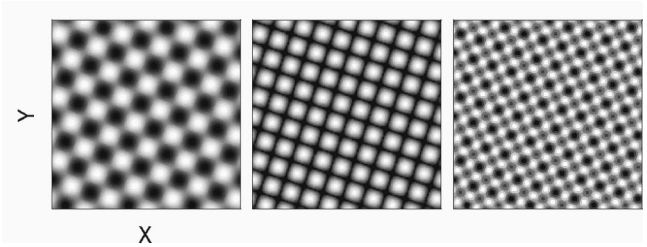

FIG. 5. Real part of the fundamental and moduli of the fundamental and second harmonics (from left to right) of a square pattern for $\Delta_A=1$, $\Delta_B=2$, $\gamma=0.5$, and $E=2.2$ (OPO,$E_c=2.062$). The moduli are in exclusive intervals [fundamental (0, 0.55), second harmonic (0.9, 1.15)]. The computing window is 45.3$\times$45.3 on a 128$\times$128 grid.

$$A_{11} = -A_{21}$$
$$= F e^{i\mathbf{k}_1\cdot\mathbf{R}} - iB_0 F^* e^{-i\mathbf{k}_1\cdot\mathbf{R}} + G e^{i\mathbf{k}_2\cdot\mathbf{R}} - iB_0 G^* e^{-i\mathbf{k}_2\cdot\mathbf{R}}$$
$$+ H e^{i\mathbf{k}_3\cdot\mathbf{R}} - iB_0 H^* e^{-i\mathbf{k}_3\cdot\mathbf{R}},$$
$$B_1 = 0, \tag{11}$$

where $\mathbf{k}_1 = (k_c, 0)$, $\mathbf{k}_2 = (k_c/2, \sqrt{3}k_c/2)$, and $\mathbf{k}_3 = \mathbf{k}_2 - \mathbf{k}_1$, instead of Eq. (5), the short-term stability is derived from an expression with the same numerator as in $\lambda_{3,4}$ with $\theta = \pi/3$. The domain of parameter space where hexagons emanate stably from the critical point is included in the corresponding domain for squares, but with $\lambda_{3,4}$ yielding lower growth rates.

In the example of Fig. 1(a) ($\Delta_B > 0$), the modulational instability terminates on the asymmetric branches at another critical value of E. This bifurcation point is subcritical, which is indicated by the existence of unstable localized structures or solitary waves on a stable plane wave background emanating from this point [cf. Fig. 1(a) for the case of stripes, i.e., solitary waves localized in one transverse direction; see also Ref. [12]]. They can be considered as residuals of the different patterns.

The above results should be compared to the scalar OPO, which behaves very similarly. It is described by the following evolution equations for the fundamental and second harmonics A and B:

$$i\frac{\partial A}{\partial T} + (L + \Delta_A + i)A + A^* B = 0,$$
$$i\frac{\partial B}{\partial T} + (\alpha L + \Delta_B + i\gamma)B + A^2 = E. \tag{12}$$

Here the symmetry breaking bifurcation described above corresponds to the threshold of down-conversion. The modulational instability sets in on the branch of steady state or plane wave solutions with $A_0 = 0$ at $E_c = \sqrt{\Delta_B^2 + \gamma^2}$ before the threshold of down-conversion, where degenerate branches with $A_0 \neq 0$ bifurcate (with A_0 a solution $-A_0$ is also a solution). As above, the critical wave number is $k_c^2 = \Delta_A$, with the fields $A_0 = 0$ and $B_0 = E/(\Delta_B + i\gamma)$ at the critical point. Starting with an expansion as given in Eqs. (4), we arrive at amplitude equations for rhombs which are similar to Eqs. (7), with the constants replaced by

$$\beta_0 = \frac{1}{\sqrt{\Delta_B^2 + \gamma^2}}, \quad \beta_j = \frac{\gamma}{\Delta_B^{(j)2} + \gamma^2}, \quad j = 1,2,3,4. \tag{13}$$

The case of rolls was extensively described in Ref. [1]. If $\beta_2 > 2(\beta_3 + \beta_4)$ they bifurcate unstably from the point where the modulational instability sets in. The behavior then seems to be similar to the case of vectorial SHG. The growth rate of the zero component of a roll solution of the amplitude equations is proportional to

$$\beta_2 - 2(\beta_3 + \beta_4) = \frac{\gamma}{(\Delta_B - 2\Delta_A)^2 + \gamma^2} - \frac{4\gamma[(\Delta_B - \Delta_A)^2 + \gamma^2 + \Delta_A^2 \cos^2\theta]}{[(\Delta_B - \Delta_A)^2 - \gamma^2 - \Delta_A^2 \cos^2\theta]^2 + 4\gamma^2(\Delta_B - \Delta_A)^2}. \tag{14}$$

From this, the domain of parameter space where square patterns emanate stably from the critical point is calculated as $(7\Delta_A - \sqrt{4\Delta_A^2 - 9\gamma^2})/3 < \Delta_B < (7\Delta_A + \sqrt{4\Delta_A^2 - 9\gamma^2})/3$. Figure 5 displays an example of a square pattern in the OPO which evolved from a randomly perturbed plane wave background. Since ReA and ImA are centered around zero, ReA is plotted also.

In conclusion, by means of a multiple scale expansion with respect to the point where the modulational instability sets in, we derived amplitude equations for different periodic patterns in intracavity vectorial SHG and the scalar OPO. In particular we determined the domain of parameter space where square patterns emanate stably from this point. The stability of square patterns was checked by means of different numerical methods (a split-step fast Fourier transform algorithm and a modified Runge-Kutta method).

[1] G. J. de Valcárcel, K. Staliunas, E. Roldán, and V. J. Sánchez-Morcillo, Phys. Rev. A **54**, 1609 (1996).
[2] G.-L. Oppo, M. Brambilla, and L. A. Lugiato, Phys. Rev. A **49**, 2028 (1994).
[3] G.-L. Oppo, M. Brambilla, D. Camesasca, A. Gatti, and L. A. Lugiato, J. Mod. Opt. **41**, 1151 (1994).
[4] K. Staliunas, J. Mod. Opt. **42**, 1261 (1995).
[5] C. Etrich, U. Peschel, and F. Lederer, Phys. Rev. E **56**, 4803 (1997).
[6] C. Etrich, U. Peschel, and F. Lederer, Phys. Rev. Lett. **79**, 2454 (1997).
[7] K. Staliunas and V. J. Sánchez-Morcillo, Opt. Commun. **139**, 306 (1997).
[8] K. Staliunas and V. J. Sánchez-Morcillo, Phys. Rev. A **57**, 1454 (1998).
[9] M. Tlidi, Paul Mandel, and M. Haelterman, Phys. Rev. E **56**, 6524 (1997).
[10] D. Leduc, M. Le Berre, E. Ressayre, and A. Tallet, Phys. Rev. A **55**, 2321 (1997).
[11] R. Martin, A. J. Scroggie, G.-L. Oppo, and W. J. Firth, Phys. Rev. Lett. **77**, 4007 (1996).
[12] C. Etrich, D. Michaelis, U. Peschel, and F. Lederer, Chaos Solitons Fractals (to be published).
[13] S. Longhi, Opt. Lett. **23**, 346 (1998).